J Solid State Electrochem (2005) 9: 254–258
DOI 10.1007/s10008-004-0608-8

ORIGINAL PAPER

J. O. Zerbino · A. Visintin · W. E. Triaca

Activation process in hydrogen storage related to oxide layers formed on zirconium alloys

Received: 19 August 2004 / Revised: 1 October 2004 / Accepted: 7 October 2004 / Published online: 10 December 2004

Abstract The passive behavior of ZrNi alloys near the rest potential is studied through in situ voltammetry, ellipsometry, and microscopic observation. A significant oxide layer growth is observed in aqueous 1 M KOH during the application of different potential programs currently used in the activation processes of the alloy. Oxide barrier effects and occlusion of hydrogen species within the film take place. The kinetics of the oxide layer formation under potential cycling plays a significant role in the activation process of metal alloys used in metal hydride batteries.

Keywords Hydrogen absorption · Zirconium and nickel oxides · Metal hydride · Batteries · Ellipsometry

Introduction

Zirconium metal is extensively used in metal hydride batteries, as the main component of AB_2 alloys due to its high hydrogen absorption capacity, as well as in biomedical applications [1–3]. Zr-based metal alloys are employed as the negative electrode of rechargeable batteries with high discharge capacities. Previous work showed that secondary phases of the Zr–Ni system contribute to improving the hydrogen absorption processes [4–8]. Two processes rule the hydrogen absorption kinetics: the rate of hydrogen diffusion in the metal, and the charge transfer rate at the metal/electrolyte interface.

Zirconium oxides, owing to their exceptional corrosion resistance, are hardly reduced during the charge–discharge cycling conditions employed in the activation of these alloy electrodes. The thermodynamic potential of the Zr/Zr oxide couple is ca. −1.6 V versus reversible hydrogen electrode (RHE), whereas for Ni electrodes the different metal/oxide couple potentials are 0.1 V and more positive over the RHE [9–12]. The charge–discharge cycling treatment applied before the alloy electrode charge is related to the formation and reduction of oxide layers on these alloys. The thin but dense and passive film on the alloy surface plays a critical role in the activation processes of the alloy electrode [1, 2]. Oxide growth is strongly dependent on the electrolyte composition and applied potentials.

In this study in order to elucidate the underlying absorption processes, voltammetry and ellipsometry are applied in situ on polished massive $Zr_{0.36}Ni_{0.64}$ alloy that catalyzes both hydrogen evolution and hydrogen bulk absorption [13]. Data analysis shows the stability and compactness of the passive layers, which are strongly dependent on the applied potential programs.

Experimental

The $Zr_{0.36}Ni_{0.64}$ alloy was obtained by melting Zr and Ni in a water cooler crucible and turned over and remelted to ensure homogeneity [1, 14]. The alloy pellet was mounted on a Teflon holder using Araldite methacrylate resin, and mechanically polished with fine grade emery paper and alumina of 1, 0.3 and 0.05 μm. The 1 M KOH solution was prepared from a.r Merck p.a. and thrice distilled water. The electrolysis cell was similar to that previously reported [15]. All electrochemical experiments were performed using a RHE in the same solution as the reference electrode. The Pt counter electrode, located in a separated compartment, was connected through a fretted glass plaque. Runs were made at 25 °C under purified N_2 gas saturation.

The optical cell was installed in a Rudolph Research type 437-02/200 B manual ellipsometer provided with a 150-W tungsten lamp and a RCA 1P21 photomultiplier.

Dedicated to Professor Gyorgy Horanyi on the occasion of his 70th birthday.

J. O. Zerbino (✉) · A. Visintin · W. E. Triaca
Instituto de Investigaciones Fisicoquímicas Teóricas y Aplicadas, Dep. de Química, Fac. Ciencias Exactas, Univ. Nac. de La Plata, C.C. 16, Suc. 4, 1900 La Plata, Argentina
E-mail: jzerbino@inifta.unlp.edu.ar
Fax: +54-0221-4254642

Data were obtained at $\lambda = 546$ nm with an incident and reflected angle of 70°. The tested optical area of about 2 mm^2 was centered on the more reflecting grain. The ellipsometric parameter Δ indicates the phase shift between the parallel and perpendicular components of the electric vector (*Es*, *Ep*) and tangent Ψ, the change in amplitude ratio of the components (*Es*, *Ep*), which result after light beam reflection.

The phase morphology of the intermetallic sample was also characterized by microscopy using a stereomicroscope (Stemi 200 Zeiss) connected to a video camera, Hitachi 220, coupled to a computer equipped with a frame grabber and image analyzer, Contron Electronics KS 300. It should be remarked that the optical measurements of the ellipsometer operating in the null mode are independent of eventual changes of intensity produced by an isolated crevice in the grain limits.

Results and discussion

Voltammetric data

Figure 1 exhibits the current/potential (*i*/*E*) voltammetric response of fresh polished Zr, Ni, and $Zr_{0.36}Ni_{0.64}$ alloy. The potential cycle is started by cathodically scanning from the open circuit potential *Eoc* down to the cathodic limit *Ec* followed by the anodic scan up to the anodic limit *Ea*. In the case of Ni the cathodic current at potentials $E < 0$ V indicates hydrogen evolution (Fig. 1a). The second cycle looks like the first one without hysteresis between anodic and cathodic scans.

In the case of Zr and depending on the potential holding time at *Ec* = −0.6 V different *i*/*E* anodic scan curves are observed in the region $-0.5 < E < 0.4$ V (Fig. 1c). This effect indicates an increase in the hydrogen evolution rate in the presence of adsorbed hydrogen that gradually accumulates in the metal/oxide interface [16].

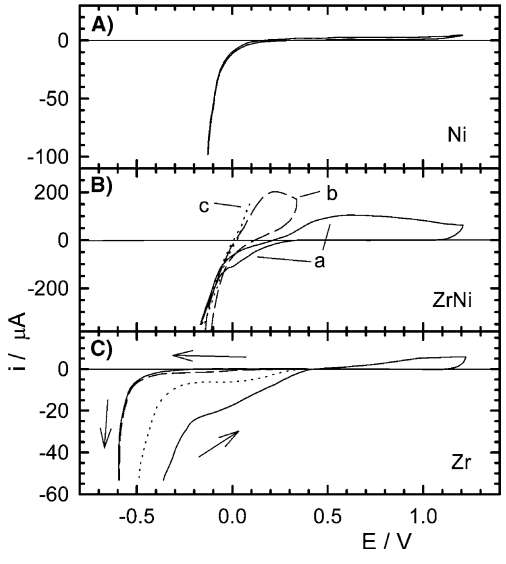

Fig. 1 *i* versus *E* plot at $v = 0.5$ mV/s from *Eoc* up to *Ec*, and cycling between *Ec* and *Ea*. **a** Ni, *Eoc* = 0.58 V, *Ec* = −0.3 V, *Ea* = 1.2 V. **b** ZrNi, *Eoc* = 0.38 V, *Ec* = −0.4 V; (a) *Ea* = 1.2 V, (b) fourth cycle after scanning between *Ec* and *Ea* = 0.3 V, (c) idem (b) using *Ea* = 0.1 V. **c** Zr, *full line* *Eoc* = 0.44 V, *Ec* = −0.6 V and holding time $\tau = 15$ min at *Ec*, *Ea* = 1.2 V, *dot line* cathodic scan of the second cycle $\tau = 0$ min

For the ZrNi alloy a cathodic current corresponding to faradaic hydrogen evolution appears in the potential region $E < 0$ V, which is similar to that observed for the Ni electrode. Otherwise, in the region $0 \text{ V} < E < 0.3$ V, the alloy shows anodic current, which corresponds to the oxidation of occluded atomic hydrogen in the oxide/metal interface. For $0.3 < E < 1.2$ V, the anodic current indicates the growth of the oxide layer. Anodic potential holding of Zr and ZrNi alloy produces the slow deprotonation of the oxide layer [17].

Ellipsometric data

Figure 2 shows the evolution of the Δ and Ψ ellipsometric parameters during potential cycling. The Ψ change is relatively small and linearly follows the Δ variation. In these conditions, the Δ decrease is directly connected with the increase in oxide layer thickness, *d* [15, 17]. In the initial region $0.4 \text{ V} < E < -0.4$ V, Δ remains nearly invariable with a value $\Delta \approx 94$. For $E > 0.4$ V, the Δ versus *E* plot shows a linear dependence. Then, during the cathodic scan, Δ remains invariable between *Ea* = 1.2 V and *Ec* = −0.4 V. Finally, the potential cycling between $-0.4 \text{ V} < E < 0.4$ V produces a new gradual Δ decrease.

Figure 3 shows the Δ change during cycling in two potential regions, namely, $-0.4 \text{ V} < E < 0.1$ V and $-0.4 \text{ V} < E < 0.3$ V. The comparison of Fig. 3a and b evidences a significantly higher Δ decrease when a higher anodic limit *Ea* = 0.3 V is imposed, in comparison to that obtained using *Ea* = 0.1 V. This indicates that the combining effect of cathodic and anodic polarization

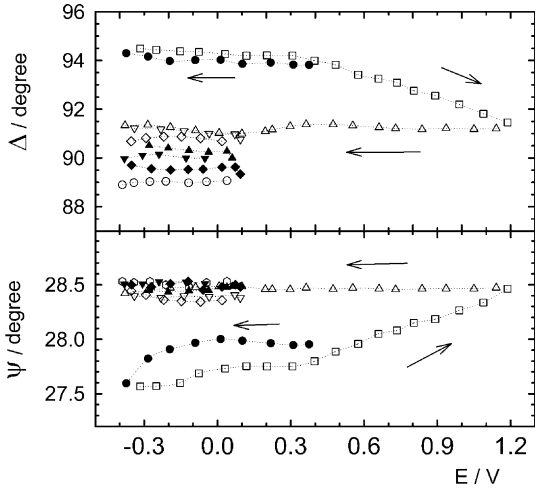

Fig. 2 Δ versus *E* and Ψ versus *E* plot for ZrNi starting the scan at *Eoc* = 0.38 V down to *Ec* = −0.4 V, then up to *Ea* = 1.2 V, and cycling between *Ec* and *Ea* = 0.1 V, $v = 0.5$ mV/s. Scanning sequence (*filled circle*, *open square*, *open triangle*, *inverted open triangle*, *open diamond*, *filled triangle*, *inverted filled triangle*, *filled diamond*, *open circle*)

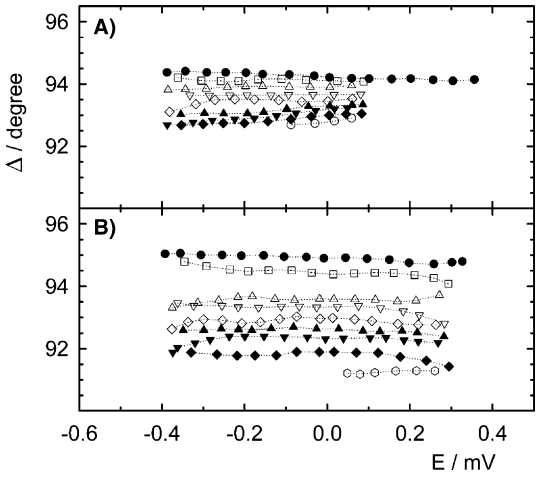

Fig. 3 Δ versus *E* plot for ZrNi starting at *Eoc* = 0.38 V, and cycling between *Ec* = −0.4 V and either **a** *Ea* = 0.1 V or **b** *Ea* = 0.3 V, *v* = 0.5 mV/s; scan sequence (*filled circle, open square, open triangle, inverted open triangle, open diamond, filled triangle, inverted filled triangle, filled diamond, open circle*)

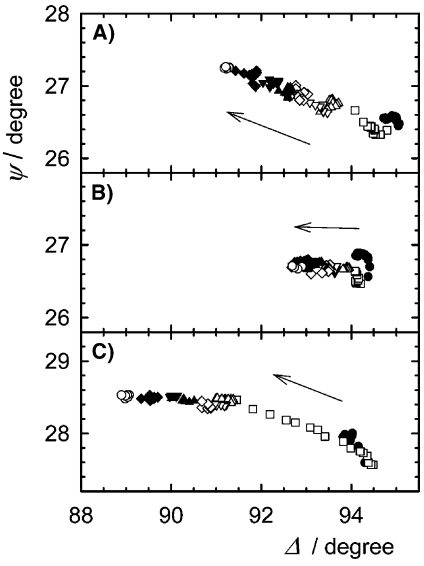

Fig. 4 Δ versus Ψ plot for ZrNi starting at *Eoc* = 0.38 V and cycling with *Ec* = −0.4 V and **a** *Ea* = 0.3 V, **b** *Ea* = 0.1 V, **c** *Ea* = 1.2 V for the first cycle and then *Ea* = 0.1 V. Scan sequence (*filled circle, open square, open triangle, inverted open triangle, open diamond, filled triangle, inverted filled triangle, filled diamond, open circle*)

produces a significant growth in the passive layer thickness, *d*. Hydrogen accumulated in the oxide matrix during cathodization appears as responsible of lower oxide passivity [17–21]. This new interfacial layer under a higher anodic polarization, *Ea*, produces a higher *d* growth.

Previously reported data show that the presence of nickel aids hydrogen access through the oxide layer. This ingress may occur by proton hopping from O^{-2} to O^{-2} in the oxide, via anion vacancies, and through easy diffusion paths such as dislocation grains and grain boundaries [17, 22]. The presence of hydrogen at high concentrations can lead to hydride induced embrittlement [23]. On the other hand, at lower cathodic polarization, hydrogen absorption may be the result of interactions between hydrogen and oxygen dissolved interstitially in the Zr lattice [25].

Figure 4 shows the Δ versus Ψ plots corresponding to the experiments already described in Fig. 2 (Fig. 4c), Fig. 3a (Fig. 4b) and Fig. 3b (Fig. 4a). The fitting of the optical data is made assuming the formation of: (1) a single homogeneous film of constant composition and different thickness, on (2) a substrate that remains during the film growth without significant changes in optical indices. This proposed schematic model allows a first estimation of thickness, compactness, and optical absorption of the interfacial layers. The program employed for the calculation uses the subroutine IBM-DFMCG in order to find the local minimum of a complex function of several variables by the method of the conjugated gradients [15]. The optical constants $n-i\,k$ (refraction index, *n*, and absorption index, *k*) were calculated unambiguously by minimizing the function *G:*

$$G = \Sigma\left(\Delta_j^{\exp} - \Delta_j^{\text{theor}}\right)^2 + \left(\Psi_j^{\exp} - \Psi_j^{\text{theor}}\right)^2 \qquad (1)$$

where *j* stands for different *dj* values.

Figure 5 shows the predicted Δ and Ψ values for the experiments of Fig. 4. A linear Δ versus Ψ relationship results when the optical indices of the layer are constant and the Δ decrease indicates an increase in thickness.

The region in Fig 4c, $94.5 > \Delta > 91.2$, is linear and fits 1.92 – i 0.0 indices. This agrees with reported values obtained for oxides grown on valve metals where the absorption coefficient $k \approx 0$ [25–28].

In this calculation the thickness of the thin passive layer spontaneously formed at open circuit is neglected, and the calculated thickness $d \approx 25$ Å corresponds to the increase in growth during cycling [17]. In a similar way, the data of Fig. 4a fits optical indices $n = 1.62$, $k = 0.077$. The analogy with the lower value of *n* observed in related systems may indicate a partial electrolyte occlusion in pores [29]. The high *k* value indicates hydrogen pen-

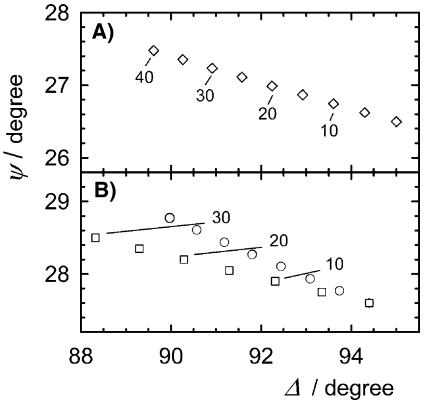

Fig. 5 Theoretical Δ versus Ψ values predicted by: **a** (*open diamond*) $n = 1.62$, $k = 0.077$ that fit Fig. 4a data, **b** (*open circle*) $n = 1.92$, $k = 0.0$ and (*open square*) $n = 2.46$, $k = 0.17$ that fit Fig 4c data. The figures indicate thickness (*d*) in Å

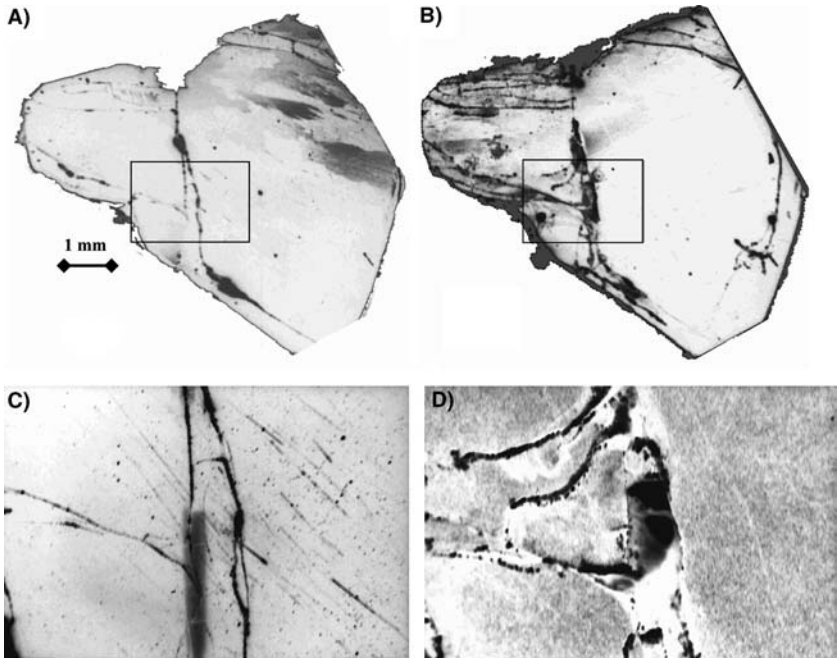

Fig. 6 Images of the $Zr_{0.36}Ni_{0.64}$ alloy, **a** before and **b** after $-0.4 < E < 0.3$ V potential cycling during $\tau = 4$ h. **c** and **d** correspond to 3.25× magnification of the surrounded area of **a** and **b**

etration in the grown composite oxide layer. Similar effects on the k index were already reported for titanium oxide layers [30].

The shift in the Δ/Ψ plot obtained for $\Delta < 91.2$ in Fig 4c indicates a change in the optical constants. The second fitted curve in Fig. 5b shows that these data may correspond to an increase in both n and k values with practically constant thickness d. However, the fitted values 2.46–0.17 of the indices seem relatively high. Probably the layer gradually grows during the cathodic cycling and optical indices may increase only partially over the initial 1.92–i 0.0 values.

For the unambiguous determination of these optical parameters and layer thickness the optical evaluation of the spontaneously formed passive layer should be necessary [31]. This needs further investigation and is outside the scope of the present work. In a similar way, the plot of Fig 4 b indicates growth and/or protonation of the initial oxide layer. Anyhow, oxide thinning under these conditions should be excluded.

Microscopic observation

The microscopic analysis of the polished alloy shows a flat surface. However, after a long electrochemical activation process the surface shows intergranular crevices around the pellet border. Figure 6 shows a micrograph of the polished electrode before and after prolonged potential cycling between $-0.4 < E < 0.3$ V. After cycling these samples were also polished with alumina 0.3 and 0.05 μm that makes the grain limit more evident. This indicates metal breaking and intergranular dissolution that take place together with oxide and hydride formation. Microscopic observation also shows an increase in the crevices after the cathodic sweep potential cycling, which indicates fragmentation of the grains and oxide growth during the activation process. More investigation is in progress on intergranular crevices in alloys prepared by the application of different remelted procedures [29].

Conclusion

The understanding of both the alloy activation process and the hydrogen absorption process is important in the strategies employed for the design of electrodes for nickel metal hydride batteries. The activation process by potential cycling increases the thickness and decreases the compactness of the passive oxide layer. The protonation of the oxide decreases the barrier effect and makes the anodic polarization more effective. Potential cycling gives rise to increasing surface oxidation, hydrogen absorption and hydride formation, and produces the consequent fragmentation of the material mainly through grain limits.

Acknowledgments This work was supported by the "Consejo Nacional de Investigaciones Científicas y Técnicas" of Argentina, the "Comisión de Investigaciones Científicas" of Pcia. Bs. As. and the "Agencia Nacional de Promoción Científica y Tecnológica". The authors thank both Dr. H.A. Peretti for supplying alloy samples and Dr. M.A. Pasquale for his collaboration in microscopy observations.

References

1. Visintin A, Peretti HA, Tori CA, Triaca WE (2001) Int J Hydrog Energy 26:683
2. Peretti HA, Visintin A, Mogni LV, Corso HL, Andrade Gamboa J, Serafini D, Triaca WE (2003) J Alloys Comp 354:181

3. Oliveira NTC, Biaggio SR, Rocha-Filho RC, Bocchi N (2002) J Braz Chem Soc 13:463
4. Harris JH, Curtin WA, Tenhover MA (1987) Phys Rev B 36:5784
5. Gebert A, Ismail N, Wolff U, Uhlemann M, Eckert J, Schultz L (2002) Intermetallics 10:1207
6. Zander D, Leptien H, Köster U, Eliaz N, Eliezer D (1999) J Non-Cryst Solids 250–252:893
7. Xiao X, Shoushi F, Guoming W, Qin H, Yuanda D (2004) J Alloys Comp 376:145
8. Bulyk II, Basaraba YB, Trostianchyn AM (2004) J Alloys Comp 376:95
9. Pourbaix M (1966) Atlas of Electrochem. Equilibria. Pergamon Press, Brussels
10. Setoyama D, Yamanaka S (2004) J Alloys Comp 370:144
11. Arroyave R, Kaufman L, Eagar TW (2002) Calphad 26:95
12. Miyake M, Uno M, Yamanaka S (1999) J Nucl Mat 270:233
13. Joubert JM, Latroche M, Percheron-Guegan A, Bouet J (1996) J Alloys Comp 240:219
14. Visintin A, Peretti EA, Corso H, Triaca WE (2003) CONAMET/SAM—SIMPOSIO MATERIA, November 2003, Bariloche
15. Zerbino JO, Gassa LM (2003) J Solid State Electrochem 7:177
16. Shibutani H, Higashijima T, Ezaki H, Morinaga M, Kikuchi K (1998) Electrochim Acta 43:3235
17. DePauli CP, Giordano MC, Zerbino JO (1983) Electrochim Acta 28:1781
18. Llewelyn Leach JS, Nehru AY (1965) Corrosion Sci 5:449
19. Oskarsson M, Ahlberg E, Södervall U, Andersson U, Pettersson K (2001) J Nucl Mat 289:315
20. Zander D, Köster U (2004) Mater Sci Eng A 375:53
21. Ramya K, Rajalakkshrni N, Sridhar P, Sivasankar B (2004) J Alloys Comp 373:252
22. Petot-Ervas G, Petot C (1990) J Phys Chem Solids 51:901
23. Svab E, Meszaros G, Somogyvari Z, Balasko M, Korosi F (2004) Appl Radiat Isot 61:471
24. Stern A, Khatamian D, Laursen T, Weatherly GC, Perz JM (1987) J Nucl Mat 148:257
25. Michaelis A, Schweinsberg M (1998) Thin Solid Films 313–314:765
26. Ord JL, De Smet DJ (1995) J Electrochem Soc 142:879
27. Patrito EM, Macagno VA (1994) J Electroanal Chem 371:59
28. Ben Amor S, Rogier B, Baud G, Jacquet M, Nardin M (1998) Mater Sci Eng B57:28
29. Urban FK, Tehrani AH, Khabari A, Griffiths P, Bungay C, Petrov I, Fim K (2002) Thin Solid Films 408:211
30. Szafranski AW (2002) J Alloys Comp 340:54
31. Meisterjahn P, Hoppe HW, Schultze JW (1987) J Electroanal Chem 217:159